JOURNAL OF MECHANICAL ENGINEERING AND SCIENCES
ISSN: 2289-4659 e-ISSN: 2231-8380
VOLUME 20, ISSUE 2, 2026, 11136 - 11148
DOI: https://doi.org/10.15282/jmes.20.2.2026.1.0869

RESEARCH ARTICLE

Thermal analysis of wavy finned heat sinks through cross-cut modifications under natural convection

Peiqi Sun[1], Mohamad Lutfie Mohamad Noor[2], Mohd Azmi Ismail[1], Ahmad Fikri Mustaffa[1]*

[1]School of Mechanical Engineering, Universiti Sains Malaysia, 14300 Nibong Tebal, Pulau Pinang, Malaysia
[2]Thermal Department, Celestica Platform and Cloud Solutions Malaysia Sdn Bhd, 11950 Bayan Lepas, Penang, Malaysia

Abstract - Wavy fin heat sinks offer significant potential for thermal management due to their enhanced surface area compared to conventional straight-fin designs. However, the effect of surface area on thermal resistance is not straightforward since thermal resistance depends on the inverse product of surface area and the convective heat transfer coefficient. This study investigates the relationship between surface area, convective heat transfer coefficient, and thermal resistance for wavy fin heat sinks under natural convection. Experimental tests were conducted on a l parallel-fin heat sink (HS1) and a wavy-fin heat sink (HS2) using a polyimide heater supplying 4 W of input power. Thermal resistance is determined from steady-state temperature measurements using three thermocouples located at the heat sink base. Despite having an approximately 10% greater surface area, HS2 exhibited a thermal resistance of 14.85 K/W, about 4.7% higher than HS1 (14.19 K/W). This highlights that increased area alone does not guarantee improved performance. This is attributed to a lower convective heat transfer coefficient (8.38 vs. 9.71 $Wm^{-2}K^{-1}$) caused by restricted airflow within the wavy fin channels. Three-dimensional steady state computational fluid dynamics simulations on four cross-cut variants of HS2 are performed to investigate the effect of geometric modifications on the convective heat transfer performance. The HS2B showed a reducing thermal resistance by up to 3% (5.57 K/W) while slightly decreasing surface area compared to HS2(16.21 K/W). These results demonstrate that effective heat sink design under natural convection requires the balancing surface area and convective heat transfer coefficient.

Article History
Received : 9 May 2025
Revised : 29 December 2025
Accepted : 15 June 2026
Published : 29 June 2026

Keywords
Natural covection
Heat sink
Heat transfer
Computational fluid dynamics
Wavy

1. Introduction

This section should provide adequate background and context for the study, explaining its significance and why it is of interest to researchers. Avoid an extensive literature review or a detailed summary of the results. The objectives of the study should be stated clearly at the end of this section. As electronic devices become more compact and powerful, thermal management is crucial to prevent overheating-induced device failure. The increasing demand for more powerful components continues to exacerbate this thermal management challenge [1]-[2]. Heat sinks have been used to dissipate undesirable heat from the electronic components to the surrounding air or, in some cases, to a liquid coolant. A common type of heat sink is the fin-type heat sink, as shown in early works [3]-[7]. Fundamental studies have shown that the thermal performance of heat sinks is strongly influenced by fin design parameters, including fin height, spacing, and thickness, as well as heat sink orientation. Prajapati [8] investigated the effects of varying fin height on the thermal performance of a microchannel heat sink using numerical simulations. Seven different fin heights, ranging from 0.4 to 1.0 mm, are compared under various operating conditions. The study shows that a fin height of 0.8 mm provided the maximum heat transfer rate and overall thermal performance. This improvement is attributed to the balance between increased surface area and the unique fluid-flow behaviour created by the open spaces between the fins and the cover. Winter and Weibel [9] investigated the effects of the height and spacing of copper fin arrays on the heat sink's heat transfer using pool boiling experiments. The experiments show that the capillary length scale (L_b) is the key length scale for heat transfer. When fin spacing or height is less than L_b, existing predictive models fail due to vapour entrapment and altered boiling regimes. This highlights the need for new predictive models to optimise heat sink designs for immersion cooling applications. Fuse et al. [10] investigated the effects of various factors on the heat transfer performance of aluminium alloy heat sinks. Factors such as fin height, thermal conductivity and emissivity are considered. The experiment utilised four finned heat sinks with varying fin heights and base thicknesses to understand their impact. For non-blackened heat sinks, the alloy's emissivity has a greater effect on the heat transfer rate than its thermal conductivity. However, when the heat sinks were blackened, heat dissipation improved due to increased thermal conductivity. When comparing both blackened and non-blackened heat sinks, it is found that increasing the fin height and base thickness consistently led to a higher rate of heat dissipation. Although increasing fin height and base thickness can improve heat transfer, these approaches may increase material usage and weight. This approach may not be desirable for compact electronic systems. Numerous studies have investigated innovative fin geometries to improve thermal performance. Ismail [11] investigated the performance of pin-fin heat sinks with unique patterns, such as cross-pin-fins, parallel-pin-fins, and double-cross-pin-fins. Based on the numerical simulations, double-cross-pin fins show the largest increase in the Nusselt number compared to other pin-fin configurations. This is attributed to the increase in surface area exposed to the flow. However, the increase in Nusselt number is counterbalanced by the increase in friction factor. This means more energy is required to move air across the fins due to the blockage. Ehsani et al. [12] investigated the effect of perforations on the performance of the pin fin heat sinks. Circular and square type perforations are added at varying positions along the pin fin height. Besides that,

***CORRESPONDING AUTHOR | A. F. Mustaffa** | ✉ afikri@usm.my

the number of perforations along the pin fin height is also varied. Numerical simulation results show that the pin fin with three square-type holes achieved the highest cooling-efficiency improvement, by 16.63%, compared to the baseline heat sink design with no pin fins. Hewage et al. [13] studied the effects of twisting angles and hole perforations on the performance of twisted-fin heat sinks. Numerical simulation results showed that a twisted fin with a 540° angle yields the greatest Nusselt number improvement compared to a standard cylindrical fin. The addition of diamond-shaped holes to the 540° twisted fin further improved the Nusselt number by 3% compared with the case without holes. Harris et al. [14] used numerical simulations and machine learning algorithms to design a biomorphic pin-fin heat sink. The scutoid fins are more efficient at reducing weight and improving heat transfer performance. Scutoid shape fins use between 6% to 14% less material while transferring 1.5 to 1.7 times more heat than standard fins. Despite these advantages, the complexity of such geometries may not be practical due to manufacturing process limitations.

Wavy and sinusoidal fin heat sinks have been studied for their potential to improve heat transfer performance. Kim et al. [15] simulated a five-waved wavy fin with a 20° corrugation angle. This study aims to find the optimal location for applying a cross-cut. The cross-cut is applied to enhance heat transfer performance by inducing flow that disrupts the thermal boundary layer. The numerical simulations show that applying the cross-cut increases the heat transfer performance by about of 24% compared to a standard wavy fin. Nilpueng et al. [16] investigated the effect of cross-cut on the thermal performance of sinusoidal wavy plate fin heat sinks. The thermal performance factor is used to evaluate heat sink performance across various fin phase shifts, air velocities, and heat sink base surface temperatures. The cross-cut heat sink with a 180° phase shift yielded the best thermal performance factor among the cases tested at Re between 500 and 2500. Wavy-fin heat sinks can be used in applications where fin height cannot be increased due to space constraints. This is because sinusoidal geometry provides a larger wetted surface area compared to straight parallel fins for the same fin height. However, the performance of wavy-fin heat sinks under fin-height limitations has not been systematically quantified. In particular, the influence of fin discretisation on natural-convection heat-transfer performance and thermal resistance remains poorly understood. Hence, the primary objective of this study is to systematically establish the relationship between thermal resistance (R), heat transfer coefficient (h), and fin surface area (A) for wavy fin heat sinks with various cross-cut configurations. Initially, the performance of parallel- and wavy-fin heat sinks is compared using experiments and computational fluid dynamics (CFD) simulations. The relationship between thermal resistance, heat transfer coefficient and fin surface area is analysed by generating 4 more wavy heat sink designs by cutting the fins into discrete sections.

2. Materials and Methods

2.1 Heat Sink Geometry

Two heat sink geometries considered for this study are shown in Figure 1. The design specifications of the heat sinks are presented in Table 1. Heat Sink 1(HS1) is a parallel fin heat sink, whilst Heat Sink 2(HS2) is wavy-finned. The heat sinks are fabricated from aluminium using a CNC machine. Due to the wavy structure, the surface area, A_s, of HS2 is larger by about 10% of HS1

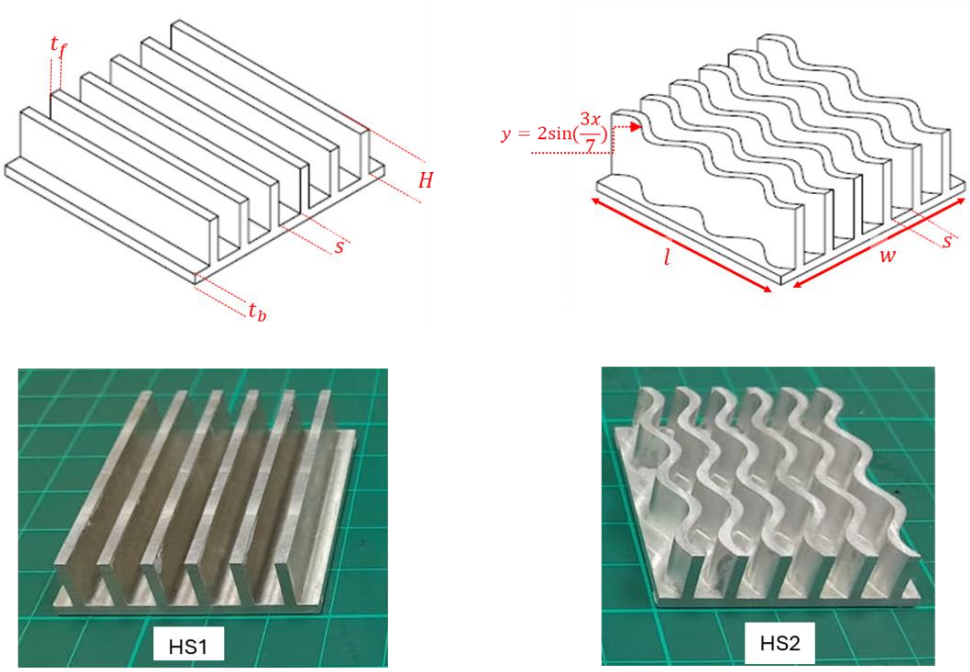

Figure 1. 1Parameters of the CNC-machined heat sink

Table 1. 1Design parameters of the heat sinks

Parameters	Parallel fin heat sink 1 (HS1)	Wavy fin heat sink (HS2)	Unit
Baseplate width (w)	44	44	mm
Baseplate length (l)	44	44	mm
Baseplate thickness (t_b)	2	2	mm
Fin height (H)	9	9	mm
Fin spacing (s)	5	5	mm
Fin thickness (t_f)	2	2	mm
Surface area (A_s)	0.007256	0.00803531	m^2

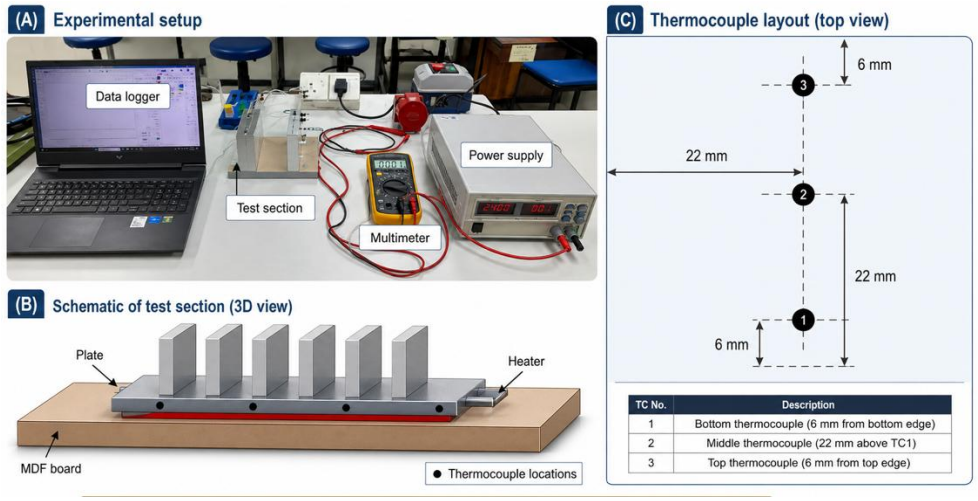

Figure 2. 2A) Illustration of the experiment setup to measure heat sink thermal performance; B) Schematic of the test section, and C) locations of the thermocouples under the heat sink

2.1.2 Experimental Setup

Figure 2(A) shows the experimental setup used to evaluate the heat transfer performance of the heat sink. This test setup is adapted from the configuration described in [17]. Medium-density fibreboard (MDF) is used as the base of the test setup. The MDF is a wood-based composite material with relatively low thermal conductivity. The MDF board is used here as a supporting base and insulating layer to minimise parasitic heat losses. A polyamide heating element is used as the heat source. The heater power (P) is fixed at 4W. The heat loss (Q_{loss}) across the MDF board is calculated using Eq. (1), where, $k, A_h, dT,$ and L correspond to the thermal conductivity of the board, the heater area, the temperature gradient across the board, and its thickness, respectively. The schematic of the test section is also shown in Figure 2(B). Five K-type thermocouples are used in this experiment. Three thermocouples are located on the heat sink base to measure the temperature (T_s). The locations of the thermocouples are shown in Figure 2(C). The temperature from each thermocouple is recorded every 5 seconds until the steady-state temperature is reached. Steady state is assumed when the temperature fluctuates by less than ± 0.5 ℃ over a continuous 5-minute period. The time to reach steady state is between 80 and 90 minutes per experiment. The base temperature (T_s) is calculated as the arithmetic average of the three thermocouple readings. One thermocouple is used to record the ambient temperature (T_∞). It is measured outside the test section and away from the immediate thermal influence of the heat sink. Another thermocouple is located under the MDF board. This temperature is used to calculate the temperature difference (ΔT) in Eq. (1). Measurement error due to external airflow is reduced by an acrylic barrier. Eq. (2) is used to calculate the heat sink heat transfer coefficient (h). Uncertainty analysis of temperature measurement is evaluated using the same method [18]. The temperature measurements are repeated 5 times. The uncertainty (U_T) shown in Eq. 3 is the root-sum -square of the instrument error (ε_B) and random error (ε_R). The instrument error ($\varepsilon_B$is specified as 0.5 °C based on the manufacturer's data. The random error (ε_R) is calculated using a standard deviation of the measured temperatures at a 95% confidence level, which corresponds to a z-value of 1.96 and a sample size (N) of 5. The standard deviation is calculated at selected time points.

$$Q_{loss}=kA_h\frac{dT}{L} \tag{1}$$

$$h=\frac{P-Q_{loss}}{A_S(T_S-T_\infty)} \tag{2}$$

$$U_T=(\varepsilon_B^2+\varepsilon_R^2)^{1/2} \tag{3}$$

2.2 Numerical Model

Heat transfer in the heat sink is simulated using a conjugate heat transfer approach in Ansys Fluent, in which heat conduction in the solid components is solved simultaneously with natural convection and surface radiation in the surrounding air. The governing equations for mass, momentum, and energy conservation are shown in Eqs. (4-6). Eq. (4) represents the mass continuity equation, where ρ and $\vec{V}$ are the density and velocity vector, respectively. Eq. (5) is the momentum equation. The left-hand side of Eq. (5) is the convective acceleration of the fluid, whilst the right-hand side is the pressure gradient, viscous term and the body force. Buoyancy effects are incorporated using the Boussinesq approximation Eq. (6), in which density variations are considered only in the gravitational body-force term of the momentum equation [20]. Here, ρ_{ref} is the reference density at reference temperature, T_{ref} and β, is the thermal expansion coefficient of the fluid, and T, is the local temperature. The β, ρ_{ref} and T_{ref} are evaluated at 292.15K. Eq. (7) is the steady state energy equation for flow, where the left-hand side represents convective heat transport by the fluid, whilst the right-hand side is the conductive heat diffusion. C_p and k are the specific heat at constant pressure and thermal conductivity, respectively.

$$\nabla \cdot \left(\rho \vec{V}\right) = 0 \tag{4}$$

$$\rho\,(\vec{V}.\nabla)\vec{V} \;=\; -\nabla p \;+\; \mu\nabla^2\,\vec{V} \;+\; \rho\,\vec{g} \tag{5}$$

$$\rho = \rho_{ref}[1 - \beta\left(\mathrm{T} - \mathrm{T}_{ref}\right)] \tag{6}$$

$$\rho\,\mathrm{C_p}\,(\nabla \mathrm{T}) \;=\; \nabla \cdot (\mathrm{k}\,\nabla \mathrm{T}) \tag{7}$$

A pressure-velocity coupling method is used to simultaneously solve the continuity, momentum, and energy equations. The second-order upwind method is used to discretise the transport equations. The PRESTO! scheme is applied for pressure interpolation at the cell faces. The flow field is laminar based on the approximated Grashof numbers of less than 10^9 [19]. Convergence of the numerical solution was assessed by monitoring the residuals and the area-averaged heat sink surface temperature. The solution was considered converged when the residuals dropped below 10^{-4}, and the change in surface temperature was less than 0.5 K. Radiation heat transfer has been modelled since radiation can contribute significantly to heat dissipation in natural convection of heat sinks. This approach has been considered by other researchers, such as in [21]-[22]. The radiation is modelled using the S2S model [20]. This model assumes that all surfaces are opaque, diffuse, and grey. View factors are computed automatically between clusters using a numerical ray-tracing method based on geometric visibility. The surface emissivity of the aluminium and MDF boards is 0.3 and 0.9, respectively. In addition, the pressure inlet and pressure outlet boundaries representing the open ambient environment are treated as radiating surfaces with a boundary temperature of 292.15 K. Conduction within the solid domains is solved using the steady-state heat diffusion in Eq. (8), where Q is the source term for internal heat generation. The source term is included to account for internal heat generation corresponding to the heater power input of 4 W.

$$\nabla \cdot (\mathrm{k}\nabla \mathrm{T}) + \mathrm{Q} = 0 \tag{8}$$

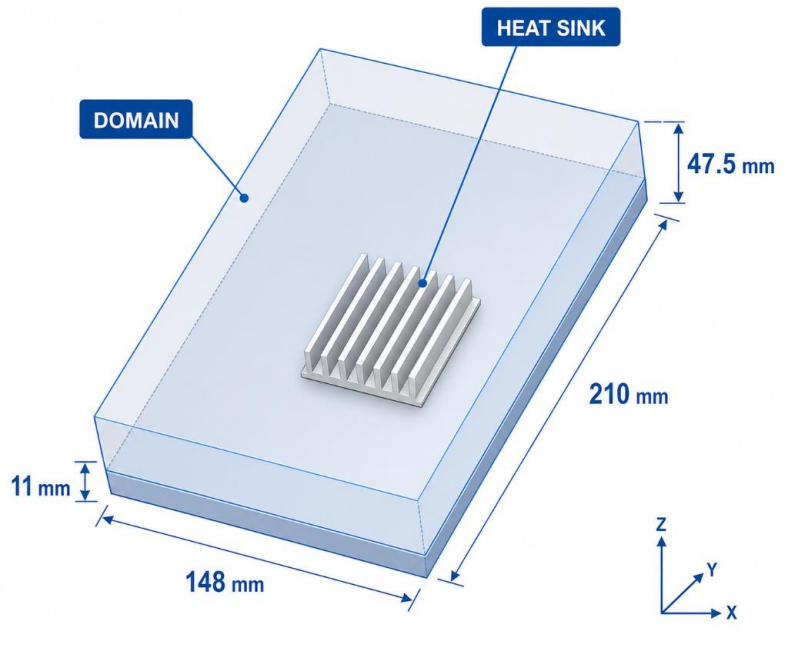

Figure 3. 3Computational domain with heat sink placement

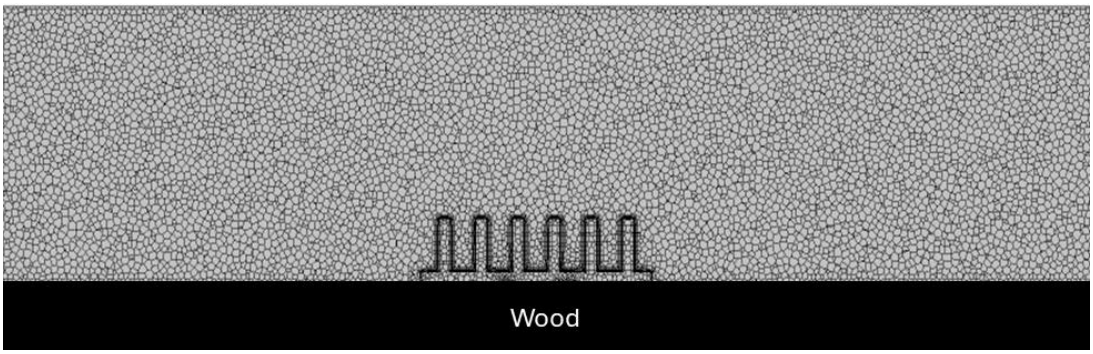

Figure 4. Mesh of the numerical domain

2.3 Computational Domain and Mesh Independence Test

Figure 3 shows the computational domain, which has dimensions of 210 mm × 148 mm × 47.5 mm. Figure 4 shows the cut view of the hexagonal grid of the computational domain. Prism layers are generated adjacent to all solid surfaces to accurately capture the near-wall velocity and thermal gradients. A mesh independence test is conducted by evaluating three different mesh resolutions: 0.5 million, 1.0 million, and 1.5 million grids. Table 2 presents the results of the mesh independence test. The area-averaged temperature measured over the heat sink's surface is compared for the three mesh resolutions. The percentage differences in heatsink temperature are computed as in Eq. (9).

$$\Delta\% = \frac{\left|T_{course} - T_{fine}\right|}{T_{fine}} \times 100\% \tag{9}$$

where T_{coarse} is the area-averaged temperature for the coarser mesh and T_{fine} is the area-averaged temperature for the next finer mesh. Increasing the mesh size has no significant effect on the area-averaged temperature measured over the heat sink's surface. Therefore, a mesh size of 1,000,000 grids is selected for the subsequent simulations to balance accuracy and computational efficiency.

Table 2. 2Comparison of the average surface temperature at three grid number levels

	Number of grids	Heatsink average temperature [K]	Δ%
Case 1	0.5 million	351.83	
Case 2	1.0 million	351.43	0.11
Case 3	1.5 million	351.50	0.02

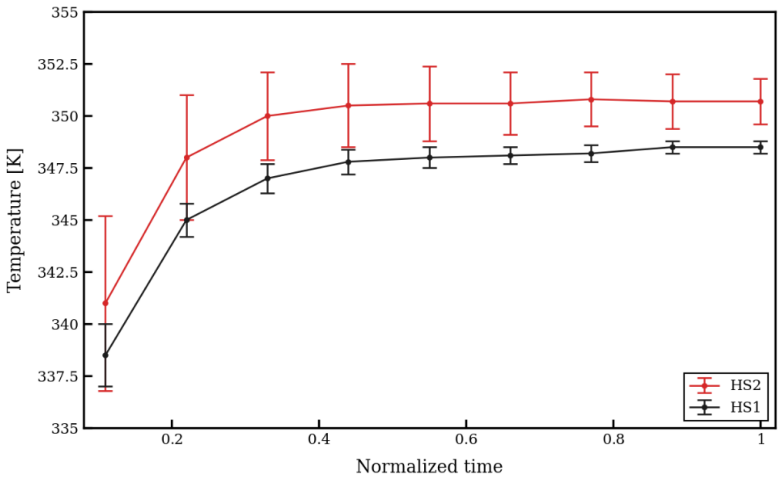

Figure 5. 4Temperature measurements at the base of HS1 and HS2

3. Results and Discussion

3.1 Comparison between Numerical and Experimental Results

Figure 5 shows the average temperature recorded by the three K-type thermocouples during the experiment for HS1 and HS2. Steady state temperature measurements are reached at about 1.5 hours. The wavy heat sink recorded a relatively higher temperature than the parallel fin heat sink. As shown in Table 3, the average heat sink base temperature of HS2 is about 0.6% higher than that of HS1. As shown in Figure 6, the CFD simulation results also show a consistent trend with the experimental data. The CFD simulation predicted the same trend as the experimental results, with HS2 having a higher surface temperature than HS1. The difference between the experiment and CFD results is within 2%. Table 4 compares the thermal resistance analysis of both heat sinks. As explained earlier, HS2 has a larger surface area of about 10.7% than

HS1. However, HS1 has a heat transfer coefficient (h) than HS2 is about 13.7% higher than HS2. Using Eq.1, the thermal resistance (R) of HS2 is higher than that of HS1 by about 4.7%. A higher thermal resistance results in the HS2 temperature being slightly higher than that of HS1. The uncertainty (U_T) of the base temperature of HS1 and HS2) is 0.57 K and 1.03 K, respectively.

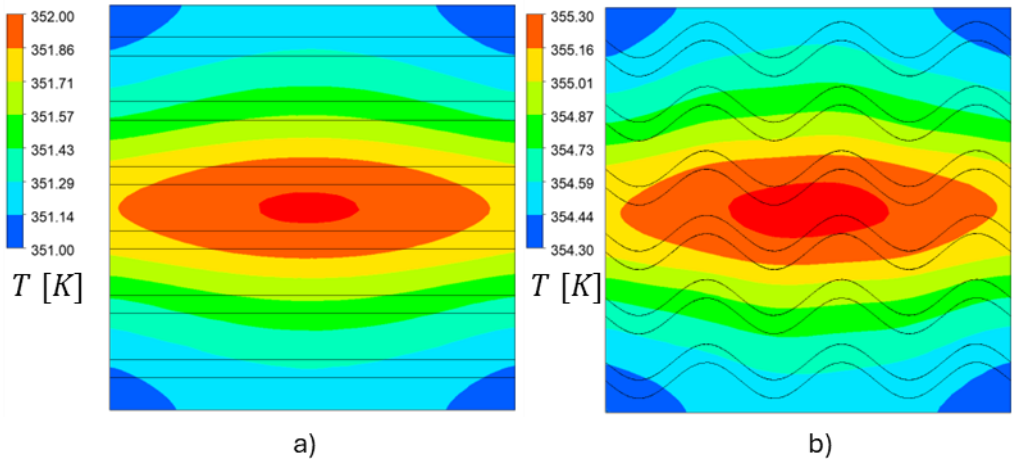

Figure 6. 5Baseplate temperature distribution of a) HS1 and b) HS2 from CFD simulation results

Table 3. 3Comparison of the averaged baseplate temperature between the experiment and the CFD simulation results

	Experiment [K]	CFD [K]	Δ%
HS1	348.44±0.31	351.51	0.88
HS2	350.62±1.03	354.82	1.2

Table 4. 4Parameters used for thermal resistance (R) analysis

Description	HS1	HS2	Unit
Baseplate Temperature, (Experiment)	348.44	350.62	K
Ambient temperature	292.15	292.15	K
Surface area	0.007256	0.00803531	m^2
Heat transfer coefficient	9.71	8.38	W/m^2K
Thermal resistance	14.19	14.85	K/W

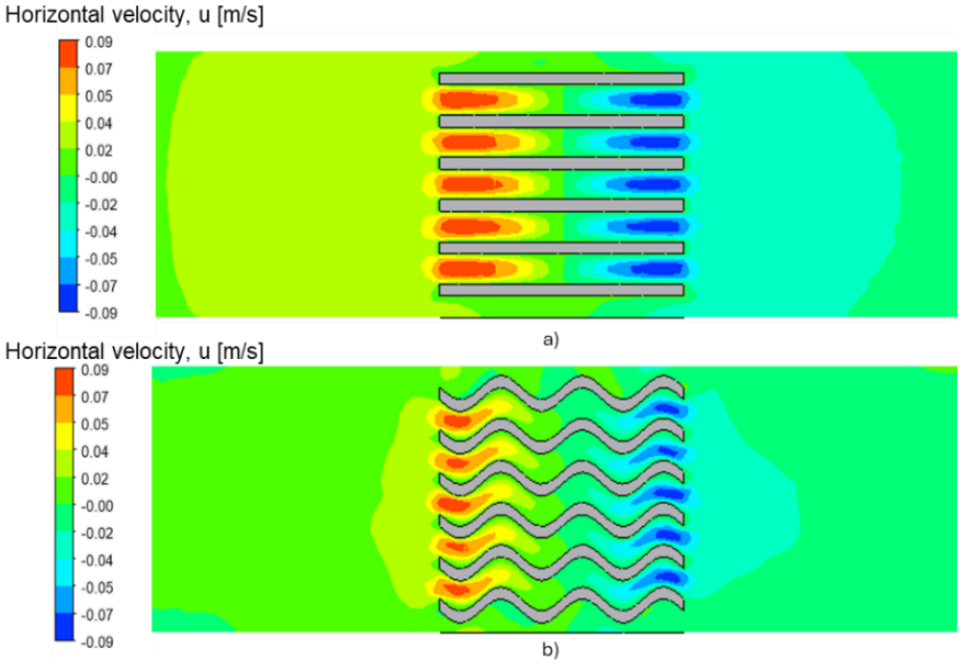

Figure 7. 6Top view of horizontal velocity contour at fin mid-height of a) HS1and b) HS2

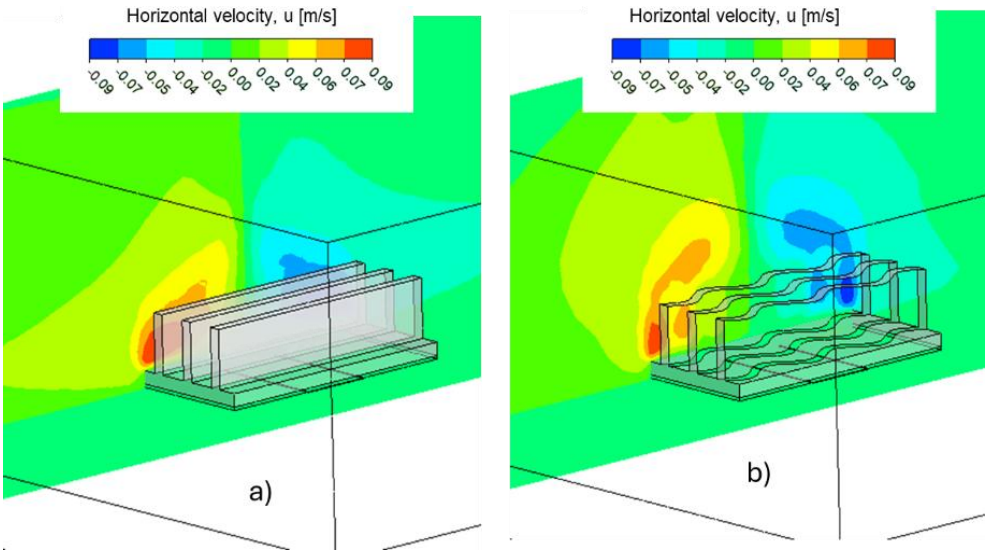

Figure 8. 7Horizontal velocity contour at midplane inside fin channel of a) HS1and b) HS2

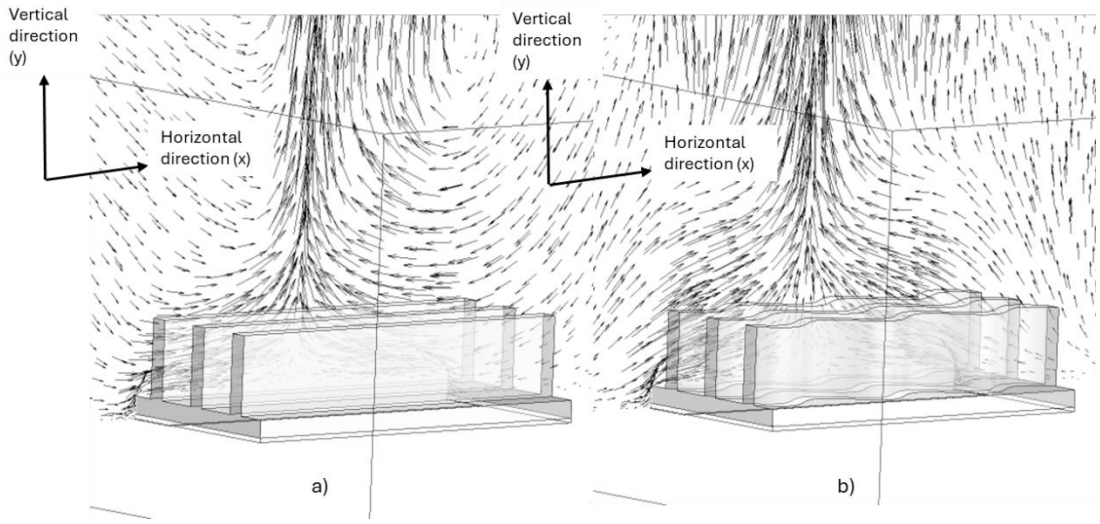

Figure 9. 8Velocity vector plotted at midplane inside fin channel of a) HS1and b) HS2

3.2 Velocity Profiles Inside Fin Channels

Figure 7 shows the horizontal velocity contour at a plane located at the mid-height of the fin. The magnitude of the horizontal velocity is high at the fin channel entrance for both HS1 and HS2. The temperature gradient between the heat sink and the ambient draws the air into the fin channel. HS1 shows a broader distribution of horizontal velocity than HS2 within the channel. Towards the heat sink centre, the horizontal velocity reduces to zero because the fluid's momentum is insufficient to overcome the buoyancy forces generated by the temperature gradient. This redirects the flow out of the horizontal fin channels, creating a chimney-like effect. Figure 8 compares the vertical distribution of horizontal velocity between HS1 and HS2. In HS1, the horizontal flow persists deeper into the channel before being redirected upward, whereas in HS2, the upward lifting occurs closer to the channel entrance. Figure 9 shows the corresponding velocity vectors at the same plane. The vectors show that the flow in HS2 is lifted more rapidly due to the higher flow resistance of the wavy fins.

The horizontal velocity profiles inside the fin channels are further analysed by plotting the velocity distributions along the lines shown in Figure 10. Here, 0 mm corresponds to the centre of the heat sink, while 5 mm, 10 mm, 15 mm, and 20 mm represent horizontal distances measured from the centre toward the channel entrance. The line located at 20 mm is closest to the fin channel inlet. Figure 11 compares the horizontal velocity profiles of HS1 and HS2 along these lines. From 5 mm to 20 mm, the maximum horizontal velocity in HS1 decreases from 0.1 m/s to 0.04 m/s, whereas in HS2 it decreases more rapidly, from 0.09 m/s to 0.02 m/s. This indicates that the wavy fin geometry in HS2 introduces higher flow resistance, causing the horizontal momentum to decay earlier within the channel. The horizontal velocity within the fin channels directly influences the heat sink's heat transfer coefficient. Higher horizontal velocities enhance convective mixing and reduce the thermal boundary layer thickness along the fin surfaces, thereby improving heat transfer. This behaviour is reflected in the thermal performance of HS1 and HS2, where HS1 exhibits a heat transfer coefficient approximately 13.7% higher than that of HS2.

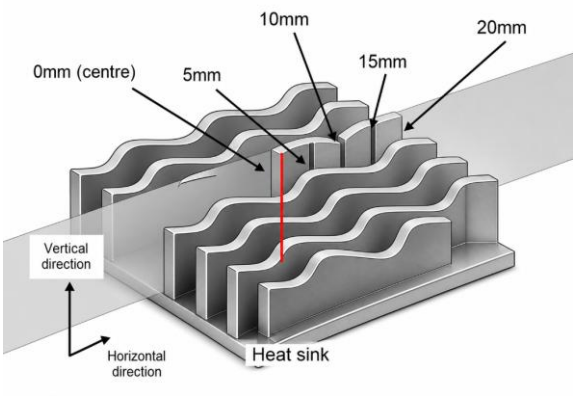

Figure 10. 9Location of midplane and lines for extracting horizontal velocity profiles inside the fin channel

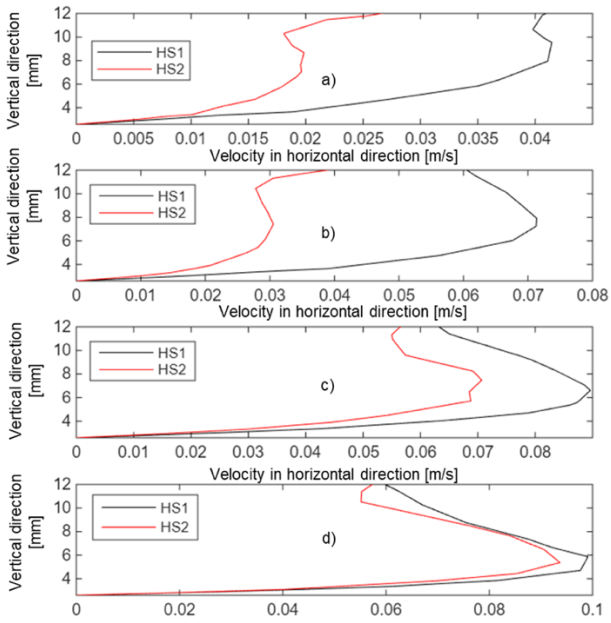

Figure 11. 10Horizontal velocity profiles inside the fin channel at a) 5 mm, b) 10 mm, c)15 mm and d) 20 mm for HS1, HS2 and HS3

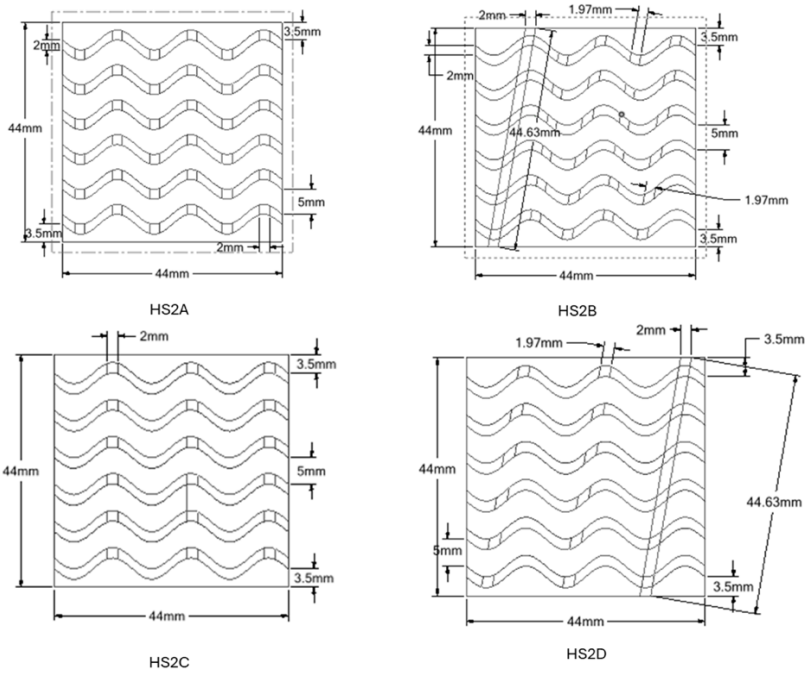

Figure 12. 11Four additional wavy heat sinks were created by cutting the continuous fins into discrete sections

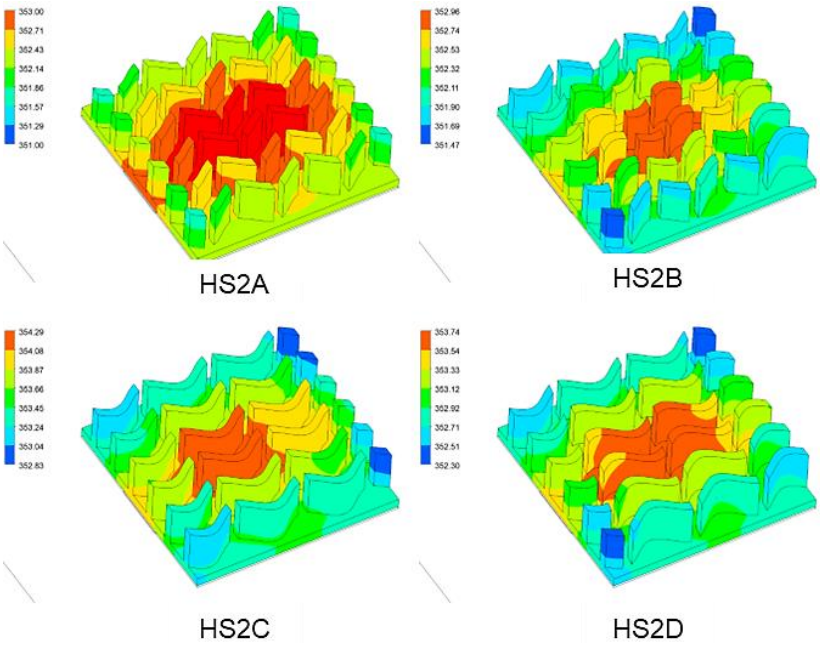

Figure 13. 12Surface temperature contour of the crosscut heat sinks

3.3 Effect of fin cross-cut on the thermal performance of wavy heat sink

As shown in the previous section, the wavy fin heat sink has slightly higher thermal resistance despite its relatively larger surface area. This shows that increasing the area does not necessarily translate to lower thermal resistance. In this section, four wavy heat sink designs are generated from HS2 by cutting the fin to create HS2A, HS2B, HS2C, and HS2D, as shown in Figure 12. HS2A and HS2C are cut parallel to the heat sink width, whilst HS2B and HS2D are slant cut across the fins. A slant angle of 80° relative to the heat sink width is selected for case HS2B and HS2D to investigate the effects of slanted cuts on heat transfer performance. This slanted angle allows a maximum of 5 slanted cuts along the fin length. Figure 13 shows the surface temperature of the heat sinks HS2A, HS2B, HS2C and HS2D. The surface temperature of each heat sink is area-averaged and is presented in Table 5. The surface temperature is used to calculate the heat sink's heat transfer coefficient using Eq. (2).

Table 5. 5Performance of the heat sinks in terms of the area-averaged surface temperature, heat transfer coefficient, surface area, thermal resistance and Rayleigh number

	HS2	HS2A	HS2B	HS2C	HS2D	Unit
h	7.677	7.982	8.160	7.828	7.986	W/m^2K
A	0.008035	0.008005	0.007869	0.00802	0.007932	m^2
R	16.211	15.651	15.574	15.929	15.786	K/W
T	354.74	352.58	352.28	353.65	353.10	K
L	0.001074144	0.000915406	0.000955417	0.000994592	0.000996494	m
Ra	2.64	1.6	1.8	2.06	2.05	-

Table 5 summarises the thermal characteristics of the baseline wavy-fin heat sink (HS2) and its four modified configurations (HS2A–HS2D). All modified designs exhibit lower thermal resistance than HS2 (16.21 K/W) despite only marginal changes in surface area. The observed performance improvement is primarily attributed to an increase in the convective heat transfer coefficient, which rises from 7.68 $Wm^{-2}K^{-1}$ for HS2 to 7.83-8.16 $Wm^{-2}K^{-1}$ for the modified geometries. HS2B achieves the highest heat transfer coefficient (8.16 $Wm^{-2}K^{-1}$) and the lowest thermal resistance (15.57 K/W). This corresponds to a 3.9% reduction relative to HS2, despite a 2.1% decrease in surface area. This improvement is accompanied by a reduction in base temperature from 354.74 K to 352.28 K. The relationship between the heat sink surface area, heat transfer coefficient and thermal resistance is shown in Figure 14. Figure 14(a) shows the relationship between surface area and heat transfer coefficient, whilst Figure 14(b) shows the relationship between surface area and thermal resistance. The abscissa is the normalised surface area, defined as the heat sink surface area divided by HS2's surface area. Normalising the surface area gives us a clearer view of how the heat sink's surface area varies relative to HS2's. Based on Figure 14, HS2B has the lowest thermal resistance among all sinks, despite its smallest surface area. The general trend observed in Figure 14a) is that reducing the surface area improves the heat transfer coefficient, thereby reducing thermal resistance. Despite having a larger surface area, HS2 has a low heat transfer coefficient, which does not reduce the thermal resistance. As discussed earlier, increasing the surface area of the heat sink alone does not necessarily contribute the reduction of the thermal resistance. One need to consider the balance between the surface area and heat transfer coefficient to improve heat sink designs.

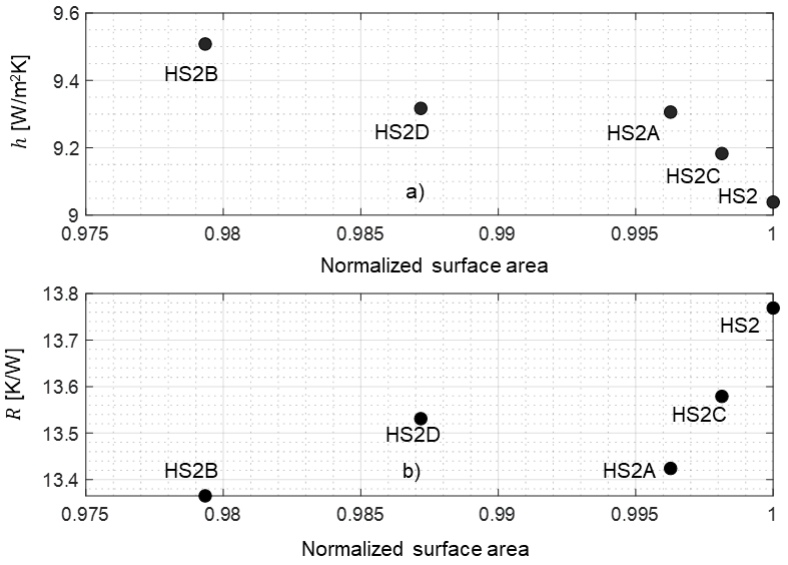

Figure 14. 13Relationship between thermal resistance, heat transfer coefficient and surface area of the heat sinks

To further investigate the influence of natural convection on the thermal performance of the heat sinks, the Rayleigh number is calculated based on Eq. (10), where g is the gravitational constant and β, is the thermal expansion coefficient of the fluid. The characteristic (L) of the heat sink is found by dividing the heat sink volume by the surface area. Kinematic viscosity, thermal diffusivity (α) and β is calculated using the film temperature $(T_f = (T - T_\infty)/2$. For laminar natural convection over horizontal surfaces, empirical and theoretical studies have shown that the Nusselt number (Nu) can be expressed as a power-law function of the Rayleigh number, $Nu = C\,Ra^n$ as shown in Eq. 11. This correlation indicates that the convective heat transfer (Nu) from a surface is strongly influenced by the buoyancy-driven flow following a power law relationship with Ra. Rearranging the relation, the heat transfer coefficient can be written as $(h \sim (k/L)Ra^n$, where k is the fluid's thermal conductivity. The constant C and the exponent n are determined empirically, and for laminar flow,n, it is typically about 0.25. The relationship between the thermal resistance (R) and Ra in Eq. (12) can be obtained by expressing the thermal resistance as $R = 1/(hA)$ in Eq. (11).

$$Ra = \frac{g\beta(T - T_\infty)L^3}{\nu\alpha} \tag{10}$$

$$Nu = \frac{hL}{k} = CRa^n \; h \sim \frac{k}{L} Ra^n \tag{11}$$

$$R \sim \frac{L}{kA} Ra^{-n}$$
$$\frac{RkA}{L} \sim Ra^{-n} \tag{12}$$

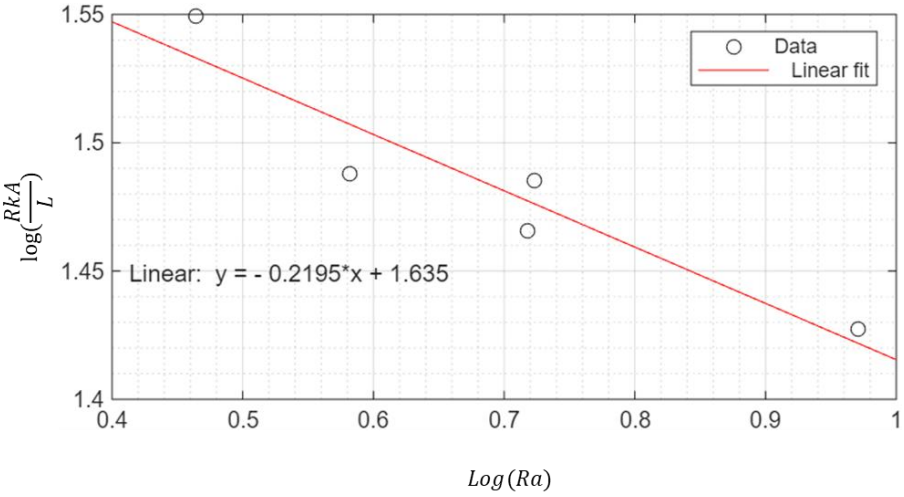

Figure 15. 14Relationship between thermal resistance and Rayleigh number

The *Ra* for each heat sink is presented in Table 5. The *Ra* quantifies the relative strength of buoyancy-driven flow compared to viscous and thermal diffusion effects. HS2 exhibits the highest Ra among the heat sinks. This indicates that

HS2 produced the strongest buoyancy-driven flow among the heat sinks. On the other hand, HS2A has the lowest Ra, about 30% lower than HS2, although the difference in surface area (A) is only 0.3%. Despite this, the heat transfer coefficient of HS2A is approximately 4% higher than that of HS2. This indicates that stronger buoyancy alone does not guarantee improved convective heat transfer, as geometric differences between HS2 and HS2A affect flow paths and surface effectiveness. Figure 15 shows the relationship between the Ra and the normalised thermal resistance (R_{norm} = RAk/L) for the five heat sinks. As shown in Eq. 12, the simulation data confirms an inverse power-law relationship between these two parameters. This means that thermal resistance decreases as the Rayleigh number increases. The exponent n, can be obtained by fitting a linear model to the data on a log-log scale, where n 0.22 is close to the typical textbook value of 0.25 for laminar natural convection over horizontal surfaces [19].

4. Conclusions

This study examines the heat-transfer performance of wavy heat sinks under natural-convection conditions. Experiments are conducted to measure the performance of two types of heat sinks: parallel-fin (HS1) and wavy-fin (HS2). Numerical simulations are conducted to further evaluate the performance of four wavy-type heat sinks. The numerical simulations show good agreement with the experiment when the heat sink base temperatures are compared. The following conclusions can be made from the study:

1) An increase in surface area does not always result in enhanced heat sink performance**.** HS2 has a larger surface area of about 10.7% compared to HS1 due to the fin's wavy structure. However, the thermal resistance (R) of HS2 is about 4.7% higher than that of HS1. This is mainly because HS1 has a lower heat transfer coefficient (h) compared to HS2 by about 13.7%. Numerical simulations show that the maximum horizontal velocity inside the HS2 fin is less than that of HS2. This contributes to a relatively lower convective heat transfer rate as compared to HS1.
2) Among the four-modified wavy-fin configurations (HS2A–HS2D), all designs reduce thermal resistance relative to the baseline HS2 (16.21 K/W), despite minor reductions in surface area. The improvements are driven by enhanced convective heat transfer coefficients, which increase from 7.68 $Wm^{-2}K^{-1}$ (HS2) to 7.83-8.16 $Wm^{-2}K^{-1}$. The best-performing design, HS2B, achieves the highest heat transfer coefficient (8.16 $Wm^{-2}K^{-1}$) and the lowest thermal resistance (15.57 K/W), corresponding to a 3.9% reduction despite a 2.1% decrease in surface area. These results confirm that improved airflow accessibility and convective effectiveness dominate thermal performance under natural convection over surface-area effects alone.
3) The Rayleigh number analysis shows that the strength of buoyancy-driven flow in horizontal heat sinks is strongly influenced by small geometric changes. HS2A exhibits a Rayleigh number approximately 30% lower than that of HS2, despite a surface area difference of only 0.3%. Specifically, HS2A exhibits a higher convective heat transfer coefficient of 7.98 $Wm^{-2}K^{-1}$ compared to 7.68 $Wm^{-2}K^{-1}$ HS2. This corresponds to a lower thermal resistance of 15.65 K/W versus 16.21 K/W, respectively. This improvement indicates that enhanced heat transfer is not governed by buoyancy strength alone but is strongly influenced by geometric features that promote more effective flow distribution and surface utilisation. Furthermore, the simulation results are supported by the inverse power-law relationship between normalised thermal resistance and Rayleigh number. The exponent $n = 0.22$ is close to the theoretical laminar value of 0.25.

Future work should focus on optimising wavy-fin geometries to enhance airflow distribution and convective heat transfer. This enables lower thermal resistance without significantly increasing surface area or material usage.

Acknowledgements

We would like to thank and acknowledge Universiti Sains Malaysia for providing facilities and funding for this project.

Funding

This work was supported by the Universiti Sains Malaysia, Research University Individual (RUI) Grant Scheme (Grant Number: R502-KR-ARU001-0000001158-K134).

Declaration of Competing Interest

The author declares no conflicts of interest.

CRediT Authorship Contribution Statement

Peiqi Sun: Methodology; Formal analysis; Validation; Investigation; Software; Writing – original draft
Mohamad Lutfie Mohamad Noor: Conceptualisation; Writing – original draft; Data curation; Methodology
Mohd Azmi Ismail: Conceptualisation; Software; Writing – review & editing; Supervision
Ahmad Fikri Mustaffa: Conceptualisation; Formal analysis; Resources; Software; Visualisation; Writing – review & editing; Funding acquisition; Project administration; Supervision

Availability of Data and Materials

The datasets generated and/or analysed during the current study are available from the corresponding author on reasonable request.

Ethics Declarations
This study did not involve human participants or animals. Ethical approval was therefore not required.

Generative Artificial Intelligence Declarations
The authors claim that artificially intelligent-assisted technologies, such as generative AI, were not used to generate content, ideas, or theories. We have just utilised AI to enhance readability and refine the language. This was used with extreme human control and oversight. The authors take full responsibility for reviewing and approving the content.

References

[1] A. R. Dhumal, A. P. Kulkarni, and N. H. Ambhore, "A comprehensive review on thermal management of electronic devices," *Journal of Engineering and Applied Science*, vol. 70, no. 1, p. 140, 2023, https://doi.org/10.1186/s44147-023-00309-2.

[2] Z. Zhang, X. Wang, and Y. Yan, "A review of the state-of-the-art in electronic cooling," *e-Prime - Advances in Electrical Engineering, Electronics and Energy*, vol. 1, p. 100009, 2021, https://doi.org/10.1016/j.prime.2021.100009.

[3] W. Elenbaas, "Heat dissipation of parallel plates by free convection," *Physica*, vol. 9, no. 1, pp. 1–28, 1942, https://doi.org/10.1016/S0031-8914(42)90053-3.

[4] C. D. Jones and L. F. Smith, "Optimum arrangement of rectangular fins on horizontal surfaces for free-convection heat transfer," *ASME Journal of Heat Transfer*, vol. 92, no. 1, pp. 6–10, 1970, https://doi.org/10.1115/1.3449648.

[5] M. H. Cobble, "Nonlinear fin heat transfer," *Journal of the Franklin Institute*, vol. 277, no. 3, pp. 206–216, 1964, https://doi.org/10.1016/0016-0032(64)90478-8.

[6] A. Brown, "Optimum dimensions of uniform annular fins," *International Journal of Heat and Mass Transfer*, vol. 8, no. 4, pp. 655–662, 1965, https://doi.org/10.1016/0017-9310(65)90051-7.

[7] A. L. London and R. K. Shah, "Offset Rectangular Plate-Fin Surfaces—Heat Transfer and Flow Friction Characteristics," *Journal of Engineering for Power*, vol. 90, no. 3, pp. 218–228, 1968, https://doi.org/10.1115/1.3609175.

[8] Y. K. Prajapati, "Influence of fin height on heat transfer and fluid flow characteristics of rectangular microchannel heat sink," *International Journal of Heat and Mass Transfer*, vol. 137, pp. 1041–1052, 2019, https://doi.org/10.1016/J.IJHEATMASSTRANSFER.2019.04.012.

[9] M. Winter and J. A. Weibel, "The Effect of Fin Array Height and Spacing on Heat Transfer Performance during Pool Boiling from Extended Surfaces," in *2022 21st IEEE Intersociety Conference on Thermal and Thermomechanical Phenomena in Electronic Systems (iTherm)*, 2022, pp. 1–7. https://doi.org/10.1109/iTherm54085.2022.9899575.

[10] H. Fuse, S. Oe, and T. Haga, "Effects of fin height, base thickness, blackening, emissivity and thermal conductivity on heat dissipation of die-cast aluminum alloy heat sink," *Metals (Basel)*, vol. 15, no. 7, 2025, https://doi.org/10.3390/met15070696.

[11] M. Ismail, "Experimental and numerical analysis of heat sink using various patterns of cylindrical pin-fins," *International Journal of Thermofluids*, vol. 23, p. 100737, 2024, https://doi.org/10.1016/j.ijft.2024.100737.

[12] H. Ehsani, F. N. Roudbari, S. S. Namaghi, p. Jalili, and D. D. Ganji, "Investigating thermal performance enhancement in perforated pin fin arrays for cooling electronic systems through integrated CFD and deep learning analysis," *Results in Engineering*, vol. 22, p. 102016, 2024, https://doi.org/10.1016/j.rineng.2024.102016.

[13] A. Hewage Dona Kalpani Rasangika, M. Shakir Nasif, and R. Al-Waked, "Numerical investigation on the thermal performance of perforated and non-perforated twisted fins at different twisting angles," *Results in Engineering*, vol. 23, p. 102332, 2024, https://doi.org/10.1016/j.rineng.2024.102332.

[14] M. Harris, H. Wu, A. Angelopoulou, W. Zhang, Z. Hu, and Y. Xie, "Heat transfer optimisation using novel biomorphic pin-fin heat sinks: An integrated approach via design for manufacturing, numerical simulation, and machine learning," *Thermal Science and Engineering Progress*, vol. 51, p. 102606, 2024, https://doi.org/10.1016/j.tsep.2024.102606.

[15] G. W. Kim, H. M. Lim, and G. H. Rhee, "Numerical studies of heat transfer enhancement by cross-cut flow control in wavy fin heat exchangers," *International Journal of Heat and Mass Transfer*, vol. 96, pp. 110–117, May 2016, https://doi.org/10.1016/j.ijheatmasstransfer.2016.01.023.

[16] K. Nilpueng, H. S. Ahn, D. W. Jerng, and S. Wongwises, "Heat transfer and flow characteristics of sinusoidal wavy plate fin heat sink with and without crosscut flow control," *International Journal of Heat and Mass Transfer*, vol. 137, pp. 565–572, 2019, https://doi.org/10.1016/J.IJHEATMASSTRANSFER.2019.03.114.

[17] P. Sun, M. A. Ismail, and A. F. Mustaffa, "Metamodel-based design optimization for heat transfer enhancement of finned heat sinks," *International Journal of Thermal Sciences*, vol. 214, p. 109896, 2025, https://doi.org/10.1016/j.ijthermalsci.2025.109896.

[18] R. J. Moffat, "Describing the uncertainties in experimental results," *Experimental Thermal and Fluid Science*, vol. 1, no. 1, pp. 3–17, 1988, https://doi.org/10.1016/0894-1777(88)90043-X.

[19] Y. A. Cengel and A. J. Ghajar, *Heat and mass transfer: Fundamentals and applications*. McGraw-Hill Professional, 2014.

[20] "ANSYS Fluent User's Guide, Release 2024 R1."

[21] I. A. Fetuga *et al.*, "Computational fluid dynamics of free convection and radiation on thermal performance of light emitting diode applications with trapezoidal-finned heat sink," *Case Studies in Thermal Engineering*, vol. 61, p. 105078, Sep. 2024, https://doi.org/10.1016/J.CSITE.2024.105078.

[22] C. H. Huang and W. Y. Chen, "A natural convection horizontal straight-fin heat sink design problem to enhance heat dissipation performance," *International Journal of Thermal Sciences*, vol. 176, p. 107540, Jun. 2022, https://doi.org/10.1016/J.IJTHERMALSCI.2022.107540.